EUROPEAN ORGANIZATION FOR NUCLEAR RESEARCH

CERN-EP/83-68
May 24th, 1983

PROTON-PROTON ELASTIC SCATTERING AT 50 GeV/c INCIDENT MOMENTUM IN THE MOMENTUM TRANSFER RANGE $0.8 < -t < 4.0$ (GeV/c)^2

Z. Asa'd[f], C. Baglin[a], R. Bock[b], J.M.Brom,[1]
L. Bugge[b,e], T. Buran[e], A. Buzzo[d], M. Coupland[f],
D.G. Davis[f], B.G. Duff[f], T. Fearnley[e,f], S. Ferroni[d],
I. Kenyon Gjerpe[b,f], J.P. Guillaud[a], V. Gracco[d],
F.F. Heymann[f], D.C. Imrie[f], K. Kirsebom[e], A. Lundby[b],
G.J. Lush[f], M. Macri[d], J.Myrheim[c,2]
M. Phillips[f], M. Poulet[a], A. Santroni[d], G. Skjevling[e],
S.O. Sørensen[e].

Annecy (LAPP)[a] - CERN[b] - Copenhagen (Niels Bohr Institute)[c] -
Genova[d] - Oslo[e] - University College London[f] Collaboration

ABSTRACT

A measurement of the proton-proton elastic differential cross-section at 50 GeV/c incident momentum in the momentum transfer range $0.8 < |t| < 4.0$ (GeV/c)^2 is presented. The data are compared to pp data at lower and higher energies, and to some model predictions.

(Submitted to Physics Letter B)

---

[1] University of Strasbourg

[2] present address NORDITA, Copenhagen

A measurement of the 50 GeV/c pp elastic differential cross-section at momentum transfer $0.8<|t|<4.0$ $(GeV/c)^2$ is presented. The experiment was part of a programme at the CERN SPS, in which hadron-proton elastic scattering was measured over a wide range of momentum transfers and beam momenta. Results on $\pi^{\pm}p$ elastic scattering at very large angles at 20 and 30 GeV/c[1], $\bar{p}p$ elastic scattering at 50 GeV/c for $0.7<|t|<5.0$ $(GeV/c)^2$[2], and $\pi^{\pm}p$[3] and $K^{\pm}p$[4] elastic scattering at 20 and 50 GeV/c for $0.7<|t|<8.0$ $(GeV/c)^2$ have already been published. Previous results on pp elastic scattering at 50 GeV/c are limited to $|t|<2.0$ $(GeV/c)^2$[5] and $|t|<1.0$ $(GeV/c)^2$[6].

The apparatus, shown schematically in Fig.1, consisted of a double-arm spectrometer downstream of a liquid hydrogen target, upon which an unseparated beam of high intensity ($\sim 1\times10^7$ ppb) was incident. The beam contained $\approx$18% protons. The beam particles were detected by a beam hodoscope consisting of three planes, each containing 40 scintillators 2mm wide. A differential Cerenkov counter (CEDAR1) on the beam line was used to identify the incident protons. The scattered particles were detected by counter hodoscopes (H1,PR1 and H2,PR2) and multiwire proportional chambers (MWPCs) in each arm, and by Cerenkov counters in the forward arm. The trigger imposed rough geometrical and kinematic constraints by means of hodoscope matrix correlations, incident beam signature requirements, and an energy threshold requirement for the forward scattered particles, imposed by an iron/scintillator-sandwich calorimeter. Veto counters surrounding the target were used to eliminate multi-particle events with tracks outside the geometrical acceptance of the experiment. Multiplicity constraints on the hodoscope matrices reduced multi-particle inelastic events. The momentum of the forward scattered particles was determined with a precision of $\pm$15% by a spectrometer magnet with an integrated field of 1.8Tm. The scattered particle trajectories were determined by nine MWPCs (CH0-CH9) with a total of 35 wire planes. Particle identification in the forward arm was provided by two threshold Cerenkov counters (C1 and C2), filled with a N_2/He gas mixture at atmospheric pressure. For both Cerenkov counters, the resulting thresholds were 8, 29 and 53 GeV/c for π, K and p, respectively.

About 6×10^5 triggers were analysed. The off-line analysis provided forward- and recoil-arm track reconstruction from the MWPC digitizings, and beam position determination from the beam hodoscope information. 3-prong vertices passing rough kinematic cuts were then fitted, using Runge-Kutta tracking through the magnetic field and applying elastic kinematic constraints. The event selection was based on the χ^2/degree of freedom (dof) of the fit, and the best vertex from each trigger was selected.

The background estimate was based on the resulting χ^2/dof distributions for each t-bin. A consistency check was provided by the coplanarity and $\Delta\theta$ distributions, the latter being the difference between the measured forward scattering-angle and the one expected for an elastic event given the measured recoil scattering-angle. For each t-bin, the number of elastic events was extracted by introducing a χ^2-cut, and subtracting the extrapolated background distribution below the cut. Clear elastic signals were seen in all t-bins. Background accounted for less than 10% for the lowest t-values, rising to a maximum of ≈30% around $|t|=1.4$ (GeV/c)^2. A total of 2303 events survived the χ^2-cuts, and 1995 elastic events were obtained after subtracting background.

The data have been corrected for angular dependent MWPC track-reconstruction efficiency and geometrical acceptance of the apparatus. Global corrections applied include random multiplicity veto, beam hodoscope efficiency, calorimeter loss, livetime, target absorption of incident beam particles, and interactions in the beam hodoscope. The overall normalization error is estimated to be less than 20%.

The pp 50 GeV/c differential cross-section measured in this experiment is shown in Fig.2, together with earlier pp 50 GeV/c data of Akerlof et al.[6]. Also shown for comparison are $\bar{p}p$ data at the same momentum[2]. Our 50 GeV/c data nicely overlap the small-$|t|$ data of Akerlof et al.. The pp and $\bar{p}p$ data, as seen from the figure, coincide in the small-$|t|$ region (< 1 (GeV/c)^2), as well as in the high-$|t|$ region (> 2.5 (GeV/c)^2). Our data feature a prominent change of slope at $|t|\approx 1.4$ (GeV/c)^2, followed by a shoulder and a subsequent fall-off in $|t|$ for $|t|>2$ (GeV/c)^2. A similar shoulder is reported by Rusack et al.[5] at the same momentum.

Fig.3 provides a comparison with pp data at lower and higher energies. The pp 24 GeV/c data of Allaby et al.[7] show a change of slope around $|t|\approx 1.3$ (GeV/c)^2, followed by a less pronounced shoulder. The apparent shift of the break-point is not a simple manifestation of Geometrical Scaling, since the total pp cross-section is virtually constant between 24 and 50 GeV/c. The higher energy data show that the 50 GeV/c shoulder has developed to a shallow dip around $|t|\approx 1.4$ (GeV/c)^2 for 100 GeV/c incident momentum[8], and to a more pronounced dip at the same $|t|$-value in the 200 GeV/c data[8,9]. The dip thus develops with increasing energy, and is seen to be very pronounced in the pp ISR data at 1064 GeV/c[10].

Several models predict the development of a dip in this t-region. A general view of diffractive models is that the dip is due to a zero in the imaginary part of the scattering amplitude, and may be filled in by the existence of a real part[11,12,13]. A real part contribution of the pp elastic scattering amplitude has been verified experimentally, being significant at lower energies ($\rho=Re(A)/Im(A) \approx -0.2$ at 50 GeV/c), while going through zero at intermediate energies ($\rho\approx 0$ at 300 GeV/c)[14].

The geometrical model of Chou and Yang[12] in the purely diffractive eikonal picture, successfully reproduces the dip structure at ISR energies, but fails to treat the lower energy dip development. Also, the model predicts a too steep fall beyond the second maximum, together with a second minimum around $|t|\approx 4$ (GeV/c)^2 (and several dips beyond), which are not seen.

An attempt to overcome these problems has been made by Bourrely, Soffer and Wu[13], whose model in the impact picture is a modified version of the C-Y model, with additional energy-dependent Regge-background. The model reproduces the low-energy shoulder, and is generally in good agreement with pp scattering data in the momentum range 14 to 2000 GeV/c. However, the $\bar{p}p$ elastic differential cross-section at 50 GeV/c calculated in this model[15] significantly disagrees with the experimental data with respect to the position of the dip, the height of the second maximum, and the slope beyond the second maximum.

The nucleon core model of Heines and Islam[16] incorporates a hard scattering mechanism, dominant at large momentum transfers, with a diffraction regime at lower transfers. The two mechanisms interfere destructively to produce the observed dip-bump structure, including the lower energy shoulder. The nucleon structure emerging from the model is that of a valence quark core surrounded by a cloud of $q\bar{q}$ sea. By fitting eight diffractive and hard parameters, experimental pp data have been reproduced in the momentum range 15 to 1500 GeV/c and over a wide t-range. The solid curve in Fig.2 shows the pp elastic differential cross-section at 50 GeV/c calculated in this model.[3] The theoretical curve provides a quantitative fit to the 50 GeV/c data, and reproduces well the shoulder. The model also describes the $\bar{p}p$ 50 GeV/c data[17], and the $\bar{p}p$ dip development it indicates agrees with recent WA7 elastic $\bar{p}p$ data

---

[3] J.P. Guillaud and M.M. Islam (private communication). Parameters used in this calculation are slightly different from those in ref.16.

at 30 GeV/c.[4]

The slope parameter $b=d/dt\ (\ln d\sigma/dt)$ of our data is found to be $2.3\pm0.1\ (GeV/c)^{-2}$ in the fall-off region $|t|>2.0\ (GeV/c)^2$. This should be compared to the $e^{1.8t}$ behaviour reported for pp scattering at $\sqrt{s}=53$ GeV[18]. It further underlines an inadequacy of diffractive models which predict too steep a fall beyond the second maximum (typically e^{6t}), as pointed out by Sukhatme[19].

The energy dependence of the pp cross-section for fixed $|t|$-values between 2 and 14 $(GeV/c)^2$ in the beam momentum range 9 to 1496 GeV/c is shown in Fig.4[6-10,18,20-28]. At any fixed value of $|t|$, $d\sigma/dt$ falls with energy, but the rate of fall decreases rapidly with increasing energy, eventually flattening out. The energy for which asymptotic behaviour is assumed to be reached seems to increase with $|t|$. An asymptotic regime is apparently reached above ≈200 GeV/c for $|t|<4\ (GeV/c)^2$. For higher t-values, asymptopia is not yet reached in this energy range. Our 50 GeV/c data are seen to lie in the energy region where the slopes start to change, while it is still possible to parametrize by a power-law of the form

$$(d\sigma/dt)_t \sim p_{lab}^{-\alpha(t)}\ ,\ p_{lab} < 50\ GeV/c,\quad |t| < 4\ (GeV/c)^2.$$

$\alpha(t)$ is found to increase roughly linearly with $|t|$. A fit yields the t-dependence

$$\alpha(t) \simeq 0.6|t| + 0.7\ .$$

At higher $|t|$-values, the same parametrization is seen to hold for smaller momenta.

Donnachie and Landshoff have suggested that a new dynamical mechanism begins to dominate in the asymptotic regime. The multiple-scattering model, involving triple gluon exchange, is a possible candidate[29]. The model predicts

$$d\sigma/dt \sim t^{-8}\ ,\ 0 \ll |t| \ll s$$

for this high-energy regime. For 50 GeV/c, well below the asymptotic domain, we find

$$d\sigma/dt \sim t^{-6.5\pm0.5}\ ,\ |t| > 2.0\ (GeV/c)^2\ .$$

---

[4] elastic $\bar{p}p$ 30 GeV/c data to be published in Phys. Lett. B.

The fixed wide-angle energy dependence of the D-L model has the form

$$d\sigma/dt \sim s^{-n} \quad , \quad n = 8 \ ^{29)}$$

for high energies, as compared to the value n=10 predicted by the Dimensional Counting Rule[30], which seems to apply to the PS energy range.

Fig.5[7,8,20,23] shows the fixed-angle energy dependence for the pp elastic cross-section at scattering angles θ_{cm} between 15° and 40°, in the momentum range 9 to 200 GeV/c. We find that a certain ratio of -t/s, corresponding to $\theta_{cm} \approx 40°$, is needed to reach a dimensional counting behaviour ($n = 9.5 \pm 0.5$) in the momentum range 10 to 24 GeV/c. For smaller scattering angles, the energy dependence is weaker.

We sincerely thank Professor M.M Islam for his valuable comments on the paper. We gratefully acknowledge the technical assistance of P. Anzoli, R.M. Audria, G. Barisone, E. Khan, R. Kiesler, J.C. Lacotte, B. Mouellic, P. Mugnier, F. Nordby, D. Ploujoux, P. Poggi, R.H. Watson, D.B. Webb, the SPS experimental support group, the DD on-line support group, the EP electronics group, and financial support from the UK Science and Engineering Research Council, the Danish National Science Research Council, the French National Centre for Scientific Research, the Italian Istituto Nazionale di Fisica Nucleare, and the Norwegian Research Council for Science and Humanities.

References

1) R. Almas et al., Phys.Lett.93B (1980) 199.
C. Baglin et al., Nucl.Phys.B216 (1983) 1.
2) Z. Asa'd et al., Phys.Lett.108B (1982) 51.
3) Z. Asa'd et al., Phys.Lett.118B (1982) 442.
4) Z. Asa'd et al., Phys.Lett.123B (1983) 265.
5) R. Rusack et al., Phys.Rev.Lett.41 (1978) 1632.
6) C.W. Akerlof et al., Phys.Rev.D14 (1976) 2864.
7) J.V. Allaby et al., Nucl.Phys.B52 (1973) 316.
8) D.H. Kaplan et al., FNAL Report, Fermilab-Pub-82/40-EXP 7120.577.
9) G. Fidecaro et al., Preprint CERN-EP/81-94 (1981).
10) E. Nagy et al., Nucl.Phys.B150 (1979) 221.
11) G.L. Kane and A. Seidl, Rev.of Modern Phys.48 (1976) 2, p.309.
12) T.T Chou and C.N. Yang, Phys.Rev.D19 (1979) 3268.
13) C. Bourrely, J. Soffer and T.T. Wu, Phys.Rev.D19 (1979) 3249.
14) K. Runge, Proc. Int. Conf. on HEP, EPS Lisbon 1981, p.328.
15) J. Soffer. Private communication.
16) G.W. Heines and M.M. Islam, Nuovo Cimento 61A (1981) 149.
G. Alberi and G. Goggi, Phys.Reports 74 (1981) 1.
17) J.P. Guillaud and M.M. Islam, University of Connecticut Preprint 80-0861 (1980).
18) H. De Kerret et al., Phys.Lett.62B (1976) 363.
19) V.P. Sukhatme, Phys.Rev.Lett.38 (1977) 124.
20) C. Baglin et al., Nucl.Phys.B98 (1975) 365.
21) J.V. Allaby et al., Phys.Lett.27B (1968) 49.
22) J.V. Allaby et al., Phys.Lett.25B (1967) 156.
23) J.V. Allaby et al., Phys.Lett.28B (1968) 67.
24) G. Cocconi et al., Phys.Rev.B138 (1965) 165.
25) G. Fidecaro et al., Nucl.Phys.B173 (1980) 513.
26) J.L. Hartmann et al., Phys.Rev.Lett.39 (1977) 975.
W. Faissler et al., Phys.Rev.D23 (1981) 33.
27) N. Kwak et al., Phys.Lett.58B (1975) 233.
28) S. Conetti et al., Phys.Rev.Lett.41 (1978) 924.
W. Faissler et al., Phys.Rev.D23 (1981) 33.
29) A. Donnachie and P.V. Landshoff, Z.Phys.C2 (1979) 55.
30) D.I. Sivers, S.J. Brodsky and R. Blankenbecler, Phys.Reports 23C (1976) 1.

Figure Captions

Fig. 1 Schematic view of the apparatus.

Fig. 2 pp elastic differential cross-section at 50 GeV/c (this exp.) compared with small-$|t|$ pp data at 50 GeV/c[6] and $\bar{p}p$ data at the same momentum[2]. Solid curve is the theoretical pp 50 GeV/c elastic differential cross-section calculated in the nucleon core model of Heines and Islam[16].

Fig. 3 pp elastic differential cross-sections at 24 GeV/c[7], 50 GeV/c (this exp.), 100 GeV/c[8] ($\times 10^{-1}$), 200 GeV/c[8,9] ($\times 10^{-2}$) and 1064 GeV/c[10] ($\times 10^{-3}$).

Fig. 4 Energy dependence of pp elastic cross-section for fixed $|t|$-values at 2, 2.5, 3, 3.6, 4, 6, 8, 10, 12 and 14 $(GeV/c)^2$ in the beam momentum range 9 to 1496 GeV/c. The solid lines are eye-fits through data points at 9 GeV/c[20], 12.1 GeV/c[21], 14.2 GeV/c[7], 16.9 GeV/c[22], 19.2 GeV/c[23], 19.3 GeV/c[22], 21.3 GeV/c[22], 24 GeV/c[7], 29 GeV/c[24], 50 GeV/c (this exp.), 100 GeV/c[6], 150 GeV/c[25], 200 GeV/c[9], 201 GeV/c[26], 282 GeV/c[27], 400 GeV/c[28], 1064 GeV/c[10] and 1496 GeV/c[18]. Some of the points are interpolations from nearby experimental points.

Fig. 5 Energy dependence of pp elastic cross-section for fixed scattering angles θ_{cm} at 15°, 20°, 30° and 40°, in the beam momentum range 9 to 200 GeV/c. The straight lines are eye-fits through data points at 9 GeV/c[20], 10 GeV/c[7], 12 GeV/c[7], 14.2 GeV/c[7], 19.2 GeV/c[23], 21.1 GeV/c[23], 24 GeV/c[7], 50 GeV/c (this exp.) and 200 GeV/c[8].

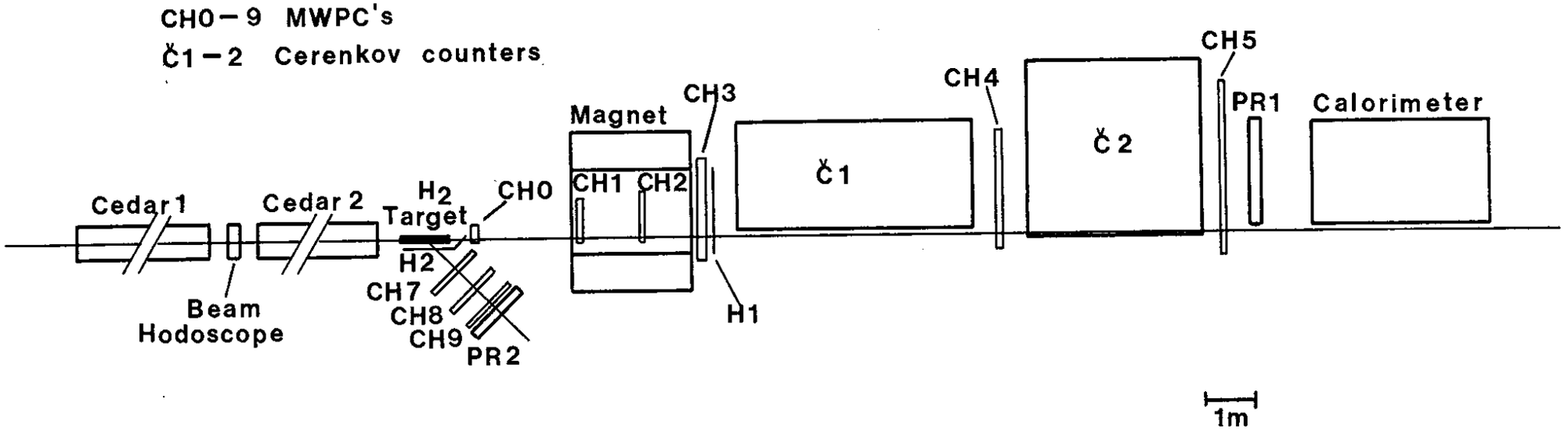
CH0 – 9 MWPC's
Č1 – 2 Cerenkov counters
Cedar 1
Cedar 2
H2
Target
CH0
Magnet
CH1
CH2
CH3
Č1
CH4
Č2
CH5
PR1
Calorimeter
Beam
Hodoscope
H2
CH7
CH8
CH9
PR2
H1
1m

Fig. 1

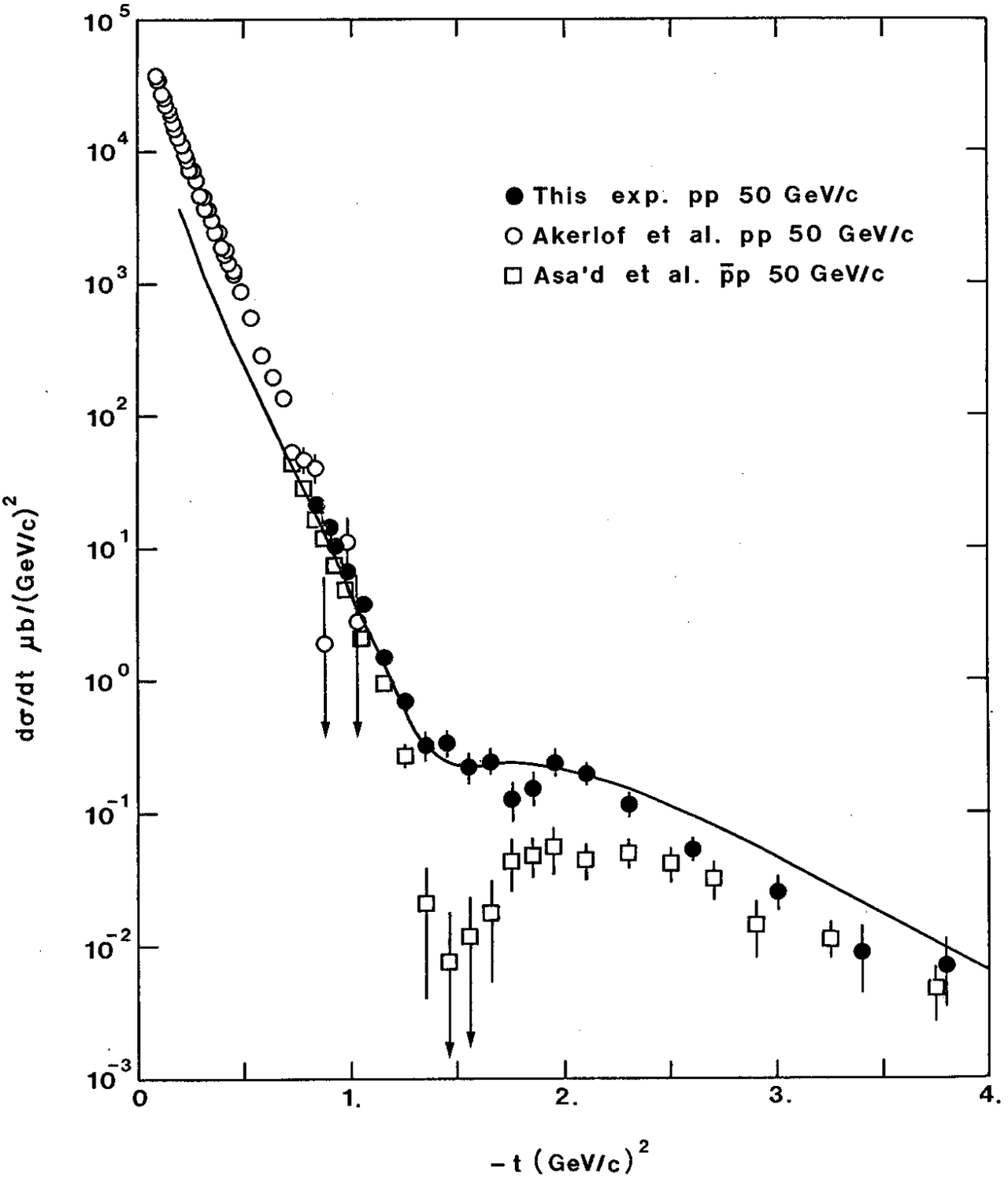
● This exp. pp 50 GeV/c
○ Akerlof et al. pp 50 GeV/c
□ Asa'd et al. p̄p 50 GeV/c
dσ/dt μb/(GeV/c)²
−t (GeV/c)²
10⁵
10⁴
10³
10²
10¹
10⁰
10⁻¹
10⁻²
10⁻³
0
1.
2.
3.
4.

Fig.2

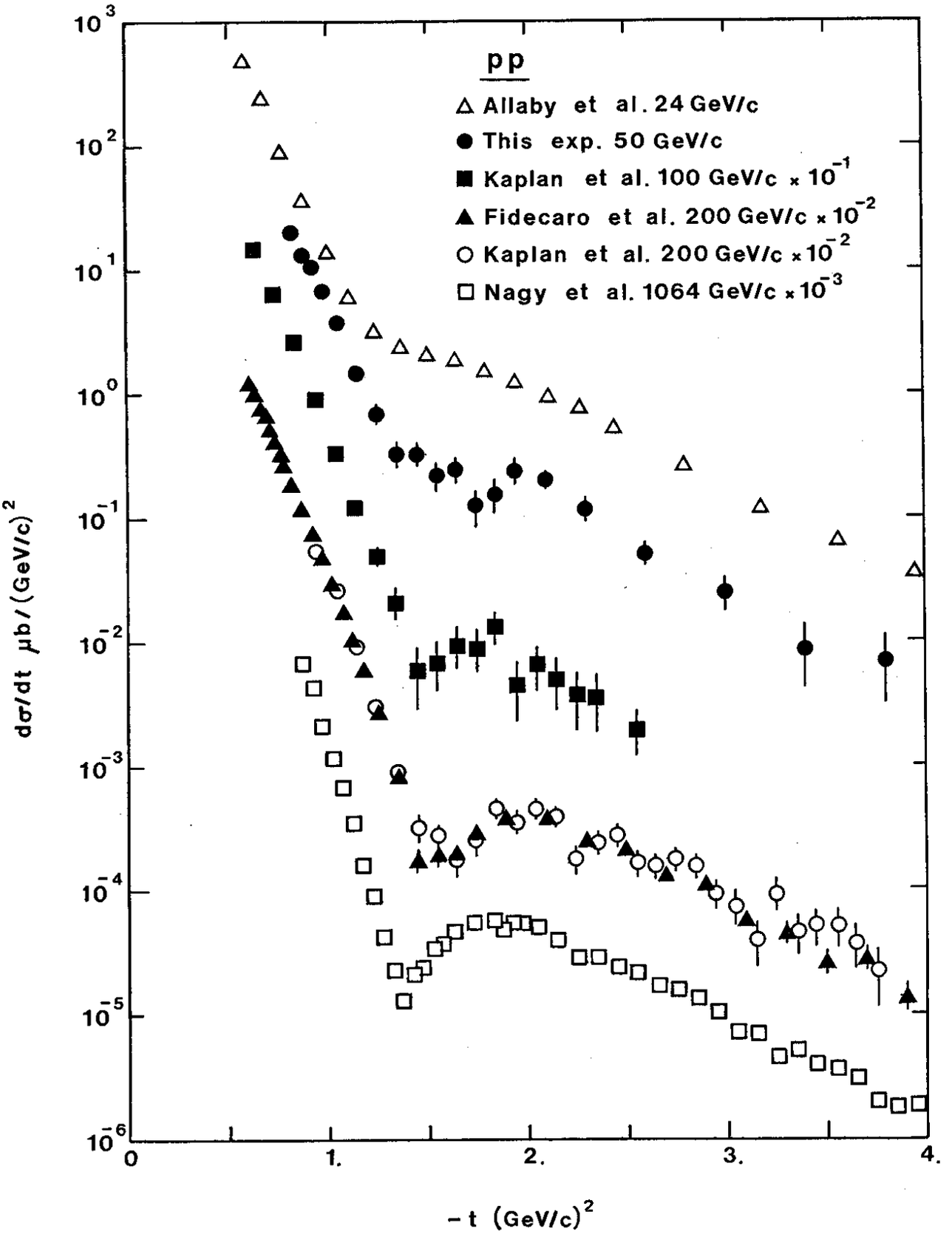
pp
Allaby et al. 24 GeV/c
This exp. 50 GeV/c
Kaplan et al. 100 GeV/c × 10^-1
Fidecaro et al. 200 GeV/c × 10^-2
Kaplan et al. 200 GeV/c × 10^-2
Nagy et al. 1064 GeV/c × 10^-3
dσ/dt μb/(GeV/c)^2
- t (GeV/c)^2
10^3
10^2
10^1
10^0
10^-1
10^-2
10^-3
10^-4
10^-5
10^-6
0
1.
2.
3.
4.

Fig.3

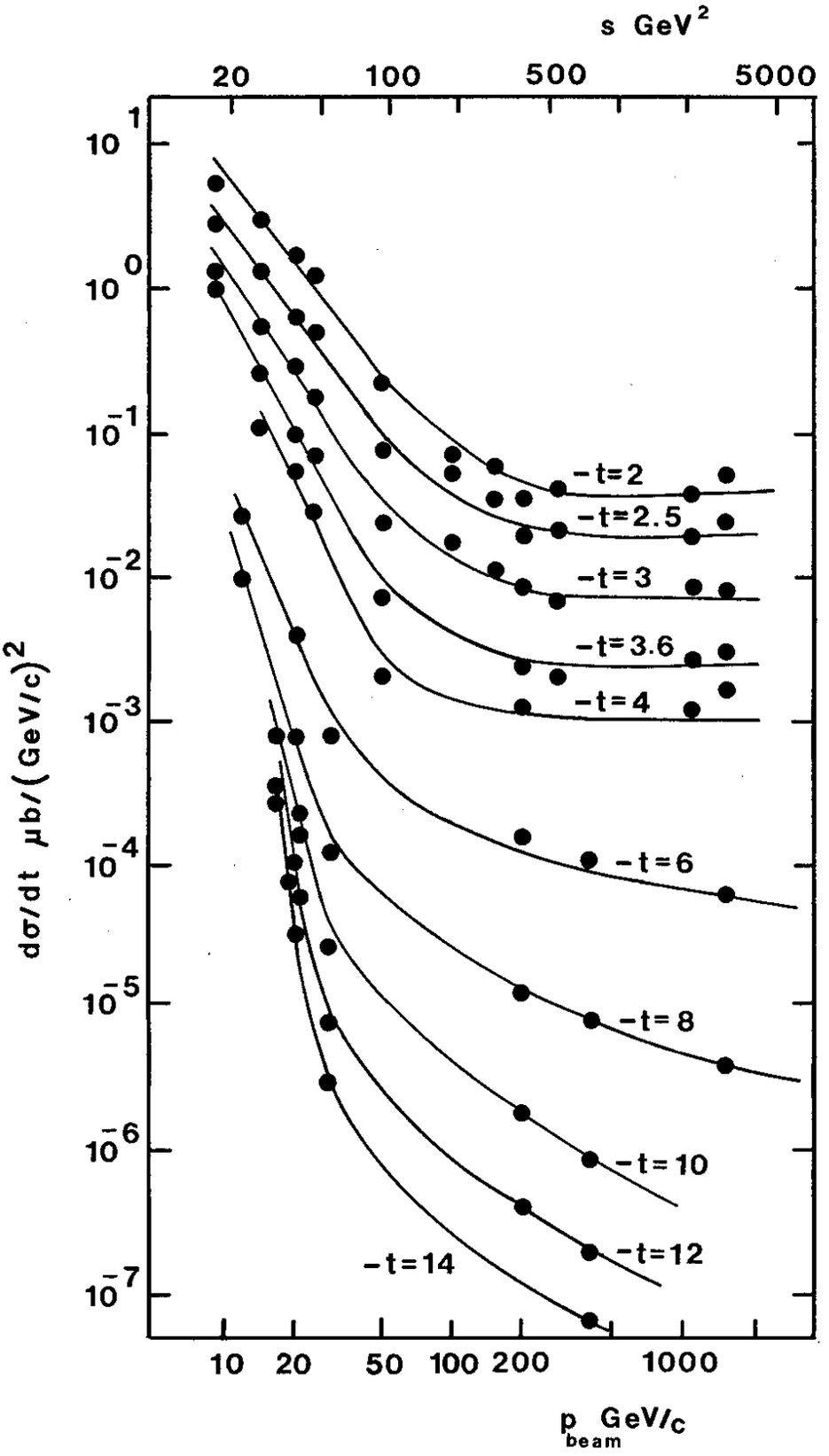
s GeV²
20
100
500
5000
10¹
10⁰
10⁻¹
10⁻²
10⁻³
10⁻⁴
10⁻⁵
10⁻⁶
10⁻⁷
dσ/dt μb/(GeV/c)²
-t=2
-t=2.5
-t=3
-t=3.6
-t=4
-t=6
-t=8
-t=10
-t=12
-t=14
10
20
50
100
200
1000
p beam GeV/c

Fig.4

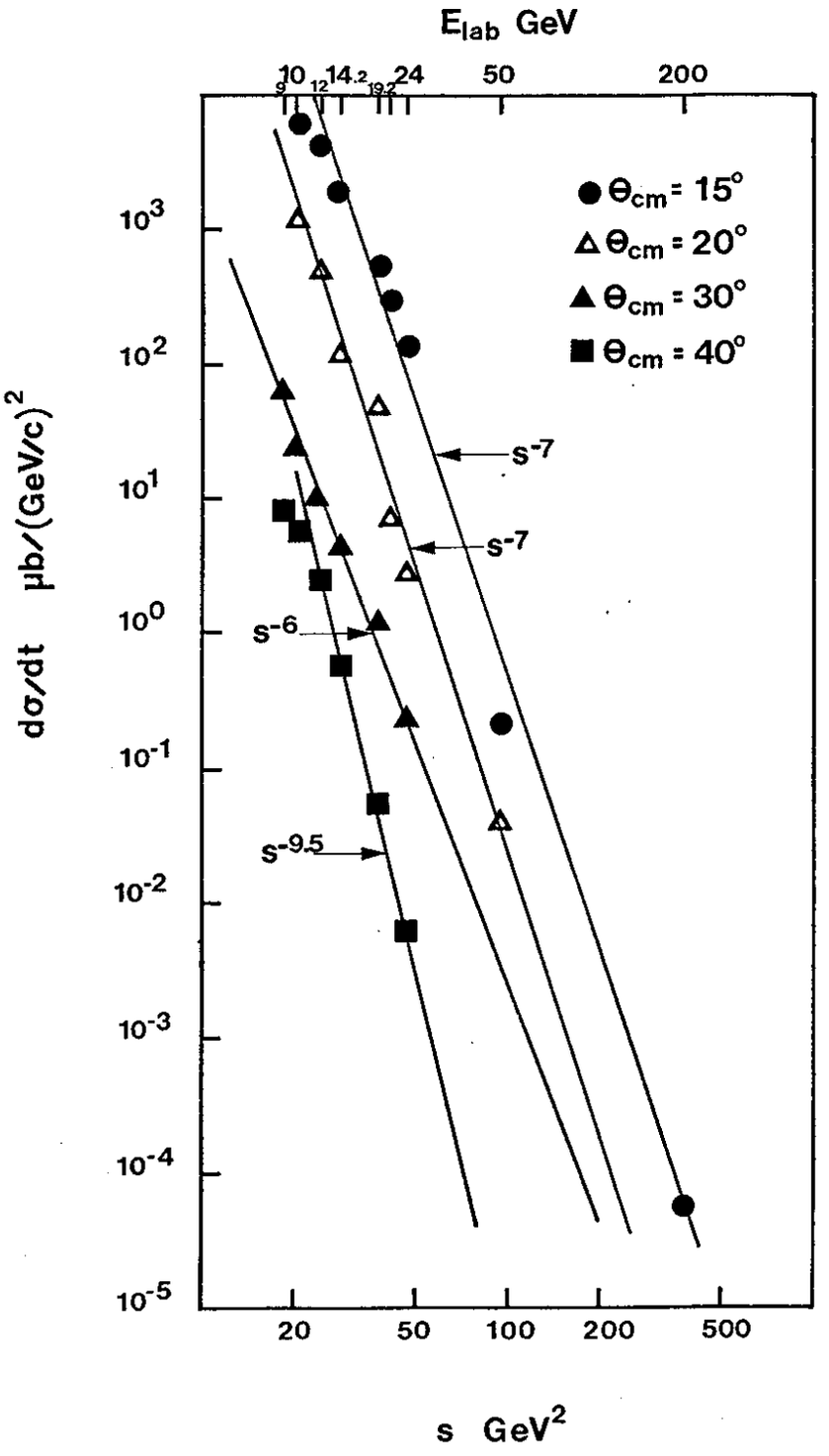
E_lab GeV
9
10
12
14.2
19.2
24
50
200
θcm = 15°
θcm = 20°
θcm = 30°
θcm = 40°
s^-7
s^-7
s^-6
s^-9.5
dσ/dt μb/(GeV/c)^2
10^3
10^2
10^1
10^0
10^-1
10^-2
10^-3
10^-4
10^-5
20
50
100
200
500
s GeV^2

Fig.5